AGU PUBLICATIONS

JGR

Journal of Geophysical Research: Oceans

RESEARCH ARTICLE

10.1002/2013JC009776

Special Section:
Pacific-Asian Marginal Seas

Key Points:
- Monsoon winds strongly affect the seasonal variation
- Interannual variability results from the weak upstream Kuroshio induced by ENSO
- 2009–2010 winter Kuroshio intrusion was stronger than that of 2010–2011 winter

Correspondence to:
Y. Yuan,
yuanyc6@163.com

Citation:
Yuan, Y., Y.-H. Tseng, C. Yang, G. Liao, C. H. Chow, Z. Liu, X.-H. Zhu, and H. Chen (2014), Variation in the Kuroshio intrusion: Modeling and interpretation of observations collected around the Luzon Strait from July 2009 to March 2011, *J. Geophys. Res. Oceans*, *119*, 3447–3463, doi:10.1002/2013JC009776.

Received 31 DEC 2013
Accepted 22 MAY 2014
Accepted article online 22 MAY 2014
Published online 5 JUN 2014

Variation in the Kuroshio intrusion: Modeling and interpretation of observations collected around the Luzon Strait from July 2009 to March 2011

Yaochu Yuan[1], Yu-Heng Tseng[2], Chenghao Yang[1], Guanghong Liao[1], Chun Hoe Chow[3], Zenghong Liu[1], Xiao-Hua Zhu[1], and Hong Chen[1]

[1]State Key Laboratory of Satellite Ocean Environment Dynamics, Second Institute of Oceanography, State Oceanic Administration, Hangzhou, People's Republic of China, [2]Climate and Global Dynamics Division, NCAR, Boulder, Colorado, USA, [3]Research Center for Environmental Changes, Academia Sinica, Taipei, Taiwan

Abstract This study analyzes the observed subtidal currents, 1/12° global HYCOM model results, and the observed time series to interpret seasonal and interannual patterns in the behavior of the Kuroshio intrusion around the Luzon Strait (LS). The observations include current measurements conducted at mooring station N2 (20°40.441′N, 120°38.324′E) from 7 July 2009 to 31 March 2011, surface geostrophic currents derived from the merged absolute dynamic topography, and the trajectory of an Argo float during the winter of 2010–2011. Results from mooring station N2 confirmed the seasonal changes in the Kuroshio intrusion and the variation of the Kuroshio intrusion during El Niño event from July 2009 to April 2010 and La Niña even from June 2010 to March 2011. The strongest Kuroshio intrusion occurs in the winter, with successively weaker currents in spring, autumn, and summer. Comparison of relative differences (Δ_{max} (*z*)) in the maximum absolute value of monthly average zonal velocity components $|U_{max}(z)|$ showed that the Kuroshio intrusion was stronger during the 2009–2010 winter (El Niño) than the 2010–2011 winter (La Niña). Furthermore, the relative differences (Δ_{max} (*z*)) in deeper layers exceed those of the surface layer. Circulation patterns in surface geostrophic currents and the Argo float trajectory confirmed the results of mooring station N2. The Kuroshio intrusion velocity variation modeled using the 1/12° global HYCOM model resembled the observation on both seasonal to interannual scales. Modeled variation in the zonal mean velocity anomaly was also consistent with Niño3, Niño4, and North Equatorial Current (NEC) bifurcation latitude indices, indicating concurrent impacts of the ENSO influence. Monsoon winds strongly affect the seasonal variation while the weak upstream Kuroshio transport induced by El Niño, strongly affects the interannual variation, such as 2009–2010 winter. In 2010–2011 winter, the impact of winter monsoon forcing still exists in the LS. However, the stronger upstream Kuroshio transport during this period did not allow the Kuroshio to penetrate into the LS deeply. This explains why the 2009–2010 winter Kuroshio intrusion (El Niño event) was stronger than that of the 2010–2011 winter (La Niña event).

1. Introduction

Studies of the Kuroshio intrusion have shown that the volume transport (VT) through the Luzon Strait, referred to as the Luzon Strait Transport (hereafter LST), occurs in a westward direction [e.g., *Qu*, 2002; *Qu et al*., 2004; *Fang et al*., 2009]. LST typically strengthens in the winter and weakens during summer months [e.g., *Qu*, 2000; *Qu et al*., 2009]. Detailed seasonal dynamics of the Kuroshio intrusion were recently described using a three-dimensional diagnostic model with modified inverse methods (MIM) [*Yuan et al*., 2007, 2008, 2009, 2012a, 2012b, 2014; *Liao et al*., 2007, 2008]. Numerical results from these investigations indicated that the northward Kuroshio current east of the LS extends downward to about 700 m, and a westward intrusion from the Kuroshio occurs above depths of 400 m in the LS [*Yuan et al*., 2007, 2008, 2009, 2012a, 2012b, 2014; *Liao et al*., 2007, 2008; *Wang et al*., 2012].

The mechanisms driving the Kuroshio intrusion into the SCS through the LS are controversial but are mostly related to the East Asia monsoon and ENSO variation, namely, there are seasonal variation due to the monsoon winds and interannual variation due to the ENSO. Previous studies have explained the influence of seasonal variation associated with monsoon forcing. For example, *Metzger and Hurlburt* [1996] showed that the pressure head created by the pileup of water from the monsoonal wind stress exerts primary controls

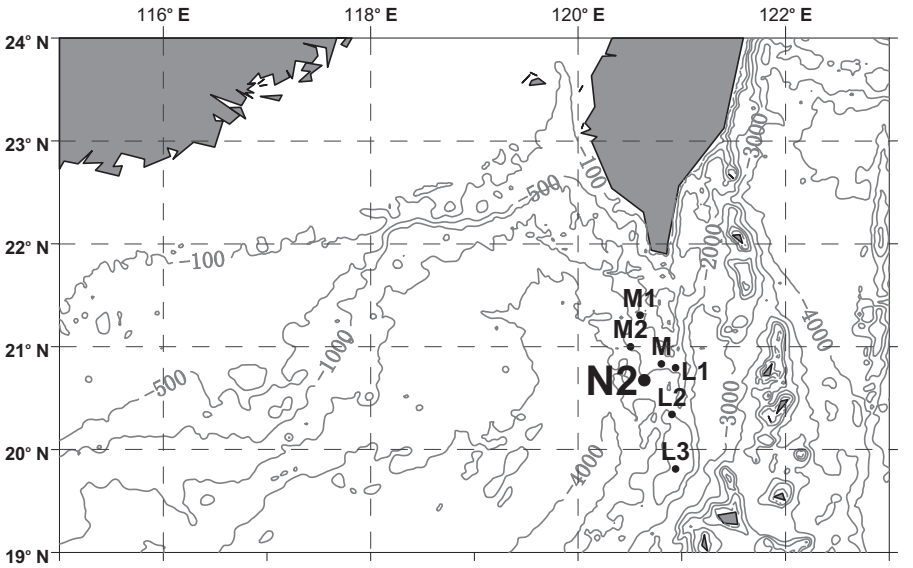

Figure 1. Location of mooring station N2 and bottom topography of the Luzon Strait and adjacent areas.

on transport variability of the Kuroshio intrusion. *Farris and Wimbush* [1996] suggested that the loop current forms when the northeast monsoon deflects the Kuroshio through the Luzon Strait. Recently, *Wu and Hsin* [2012] empirically validated the wind patterns that regulate the intrusion using a three-dimensional ocean model. Their study showed that the winds within the SCS have a greater influence on the intrusion than those outside the SCS.

Other studies have examined the influence of ENSO on the interannual variability. First, *Sheremet* [2001] discussed the variation of the Kuroshio intrusion into the LS as a function of upstream Kuroshio transport, describing different scenarios by which the Kuroshio may either penetrate or leap the strait. The mechanisms outlined by *Sheremet* [2001] depend on the nondimensional half-width of the gap, $\gamma = a\,(\beta/A_l)^{1/3}$, where $2a$ is the gap width (i.e., the width of the LS here), $\beta = df/dy$ (called the β effect), and A_l is the lateral viscosity coefficient. The Kuroshio intrudes in the case of sufficiently large γ. In this scenario, flows enter the gap and extend westward. In the case of small γ, the current "leaps" the gap effectively bypassing the strait. The Reynolds number ($\mathrm{Re} = Q/A_l$, where Q is the VT) can also affect the intrusion. Weak upstream Kuroshio transport (corresponds to low *Re*) enhances the intrusion due to inertia effects. Some other studies have also framed the influence of El Niño and La Niña events on the Kuroshio intrusion. *Qiu and Lukas* [1996] pointed out that the North Equatorial Current (NEC) in the La Niña years generally bifurcates at a lower latitude. *Kim et al*. [2004] also showed that the bifurcation point for the NEC east of the Philippines shifted northward during El Niño, and southward during La Niña. The northward shift of the NEC bifurcation occurred due to a strong Mindanao Dome in associated with a weak Kuroshio transport during El Niño years [*Masumoto and Yamagata*, 1991; *Qu et al*., 2004]. The weak upstream transport associated with ENSO events therefore exerts the interannual influences on the Kuroshio intrusion [also see *Yaremchuk and Qu*, 2004]. *Yuan et al*. [2012a] suggested that westward VT of the Kuroshio intrusion across the upper layer of the LS relates to El Niño and La Niña phenomena, with higher VT during El Niño events, relative to that of La Niña. The above results had been identified by the observations. For example, the LS was dominated by southeasterly wind in summer, which could not drive the Kuroshio intrusion into the SCS. Based on the Ocean Acoustic Tomography (OAT) with ADCP experiments, conducted from May to September 2008 (the final phase of the 2007/08 La Nina) in the LS, *Taniguchi et al*. [2010] indicated that the Kuroshio did not intrude into the SCS through the Luzon Strait during summer 2008. This is because the bifurcation point for the NEC shifted southward and the stronger upstream transport associated with the final phase of the 2007/08 La Nina. However, based on the comparisons of current trajectories observed using Argo, mooring stations and theoretical model analysis, *Yuan et al*. [2014] confirmed a summer Kuroshio intrusion through the LS in summer 2009. This summer Kuroshio intrusion resulted from the weak upstream Kuroshio transport in

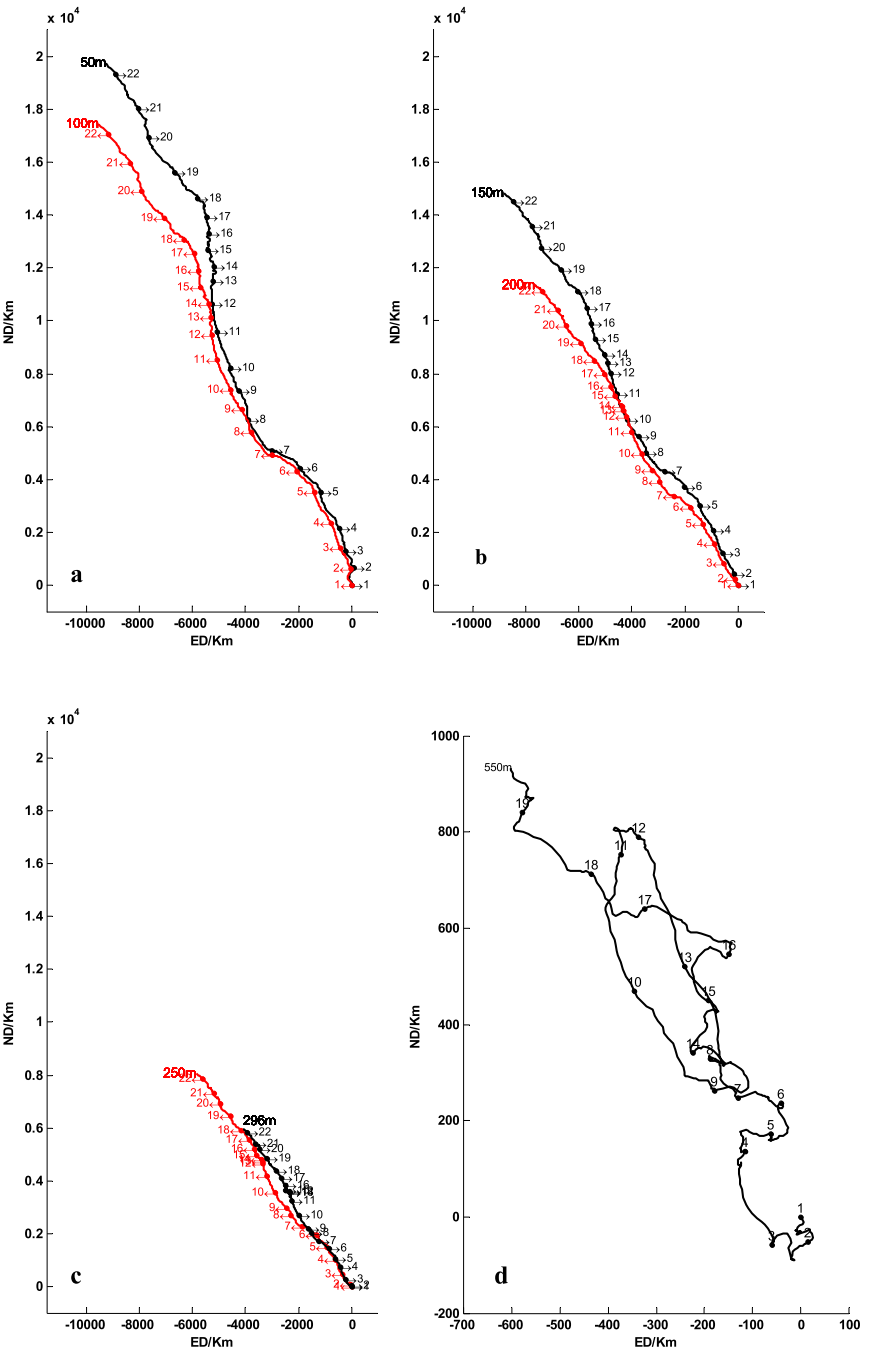

Figure 2. Progressive vector diagrams of observed daily subtidal currents with the tidal signal removed using a 40 h Chebyshev II low-pass filter. Currents measured at (a) 50 and 100 m, (b) 150 and 200 m, (c) 250 and 296 m, (d) 550 m by mooring station N2, from 7 July 2009 to 10 April 2011. The numbers indicate observation date. (1) 7 July 2009; (2) 1 August 2009; (3) 1 September 2009; (4) 1 October 2009; (5) 1 November 2009; (6) 1 December 2009; (7) 1 January 2010; (8) 1 February 2010; (9) 1 March 2010; (10) 1 April 2010; (11) 1 May 2010; (12) 1 June 2010; (13) 1 July 2010; (14) 1 August 2010; (15) 1 September 2010; (16) 1 October 2010; (17) 1 November 2010; (18) 1 December 2010; (19) 1 January 2011; (20) 1 February 2011; (21) 1 March 2011; (22) 1 April 2011 (ED: Eastern distance, ND: Northern distance).

summer 2009 affected by the ENSO due to the inertia effects [*Yuan et al.*, 2014]. It is worthy to note that there exists additional decadal scale influence on the variation of the Kuroshio intrusion and its connection between NEC bifurcation latitude as well. Thus, the variation of the Kuroshio intrusion and its connection between NEC bifurcation latitude are not necessarily the same ranging from the seasonal to interannual to decadal scales [refer to *Qiu and Lukas*, 1996; *Qiu and Chen*, 2010].

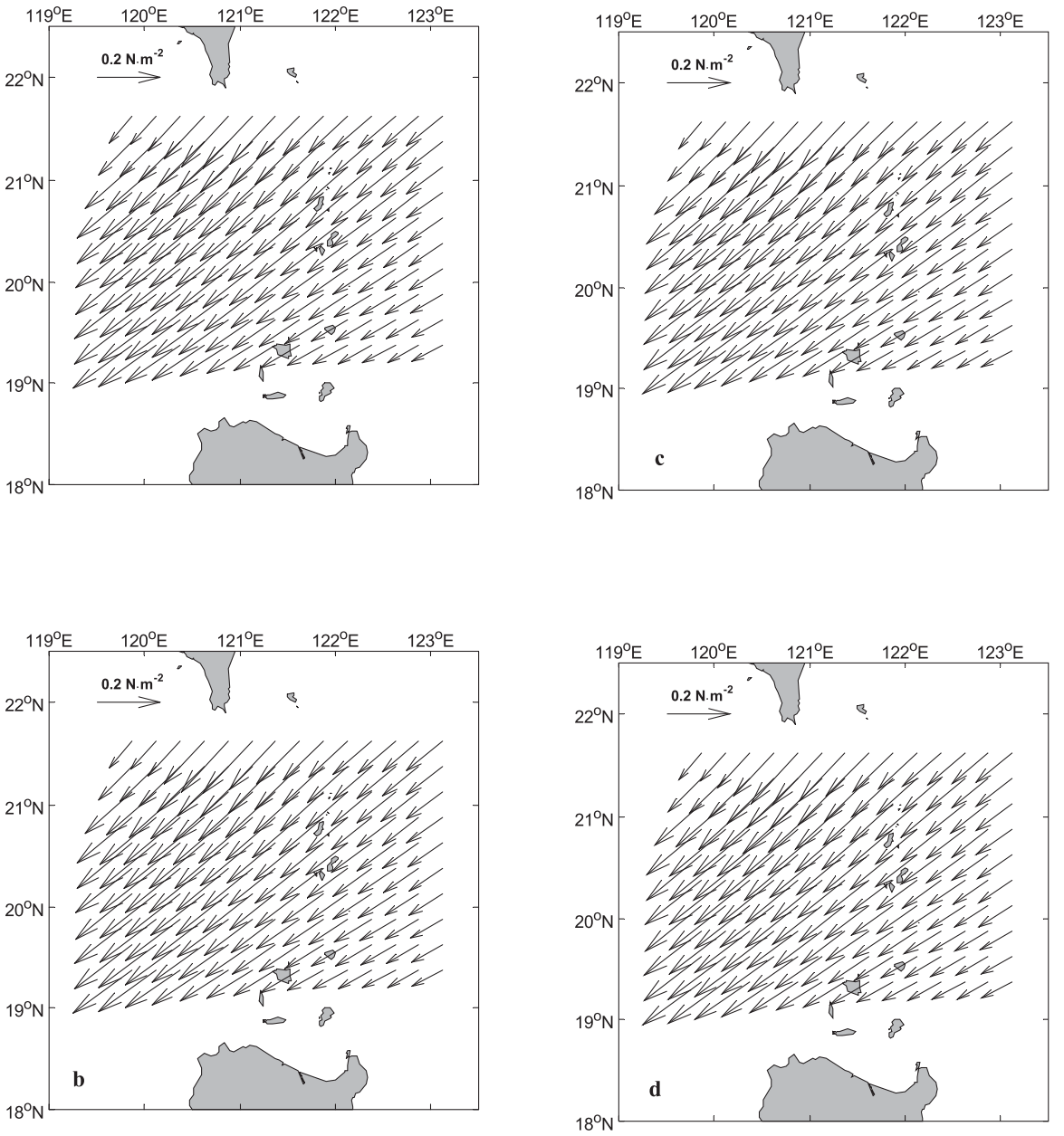

Figure 3. The average wind stress (N/m^2) distribution in the study area during (a) December 2009, (b) January 2010, (c) December 2010, and (d) January 2011.

There are also several direct current measurements to monitor the current dynamics in the SCS. Three acoustic Doppler current profilers (ADCPs) were deployed at L1, L2, and L3 sites (see Figure 1) along the Heng Chun Ridge in the central Luzon Strait from 1997 to 1999 [*Liang et al.*, 2008]. The observed current indicated that the Kuroshio intrusion consistently flowed into the SCS through the central LS (about 20°20′–20°50′). A current mooring system was deployed at M site (Figure 1) from March to April 2002, and both observed and modeled currents showed that the Kuroshio intrusion flowed into the SCS through the central LS [*Yuan et al.*, 2008]. Based on the observed results from the Long Ranger 75 K and 150 K, ADCPs deployed at two mooring stations, M2 and M1 (see Figure 1) from 25 April to 8 October 2008, the observed subtidal currents and the modeled currents both indicated that (1) a part of the Kuroshio intrusion flows northwestward through the upper layer at section 120°36′E between 20°20′N and 21°20′N in the LS during the spring

Table 1. Monthly Average Velocities for Subtidal Currents $\vec{v}(z,m,y)$ in the Upper 296 m, as Measured by ADCP Sensors at Mooring Station N2 From 7 July 2009 to 31 March 2011

		Year	Jan	Feb	Mar	Apr	May	Jun	Jul	Aug	Sep	Oct	Nov	Dec
50 m	U	2009							3.7	−11.2	−9.7	−25.7	−29.7	−39.8
		2010	−33.4	−15.0	−11.2	−19.5	−7.4	1.3	1.1	−8.0	0.6	−2.4	−13.8	−31.5
		2011	−37.8	−15.4	−31.9									
	V	2009							31.2	22.7	33.1	51.1	34.4	26.1
		2010	42.6	46.4	32.5	51.8	40.4	32.7	20.1	23.3	24.7	23.1	26.8	36.4
		2011	49.8	46.4	47.8									
100 m	U	2009							−1.0	−15.0	−13.4	−23.6	−25.5	−35.0
		2010	−29.7	−14.6	−14.8	−19.5	−8.2	−1.1	−2.6	−12.2	−2.9	−5.8	−15.6	−27.8
		2011	−31.3	−17.9	−30.6									
	V	2009							29.0	29.0	36.6	43.0	31.5	22.6
		2010	32.2	34.9	28.0	43.6	35.0	25.9	19.1	24.1	24.5	23.6	20.7	30.1
		2011	38.6	43.7	40.7									
150 m	U	2009							−5.7	−16.2	−14.2	−19.6	−21.8	−27.6
		2010	−26.5	−12.0	−15.6	−15.5	−8.7	−4.0	−5.1	−13.2	−5.9	−5.7	−14.1	−23.1
		2011	−26.9	−15.1	−27.1									
	V	2009							19.8	28.7	34.1	35.5	26.8	22.2
		2010	26.0	24.8	23.4	38.0	29.1	15.7	11.5	22.0	22.5	22.9	23.5	30.7
		2011	30.8	33.5	35.7									
200 m	U	2009							−4.9	−15.4	−14.8	−15.2	−18.5	−23.5
		2010	−20.7	−10.3	−15.0	−14.8	−8.2	−3.4	−2.8	−9.9	−5.8	−7.9	−15.5	−19.6
		2011	−20.9	−12.5	−22.3									
	V	2009							10.6	21.5	29.9	26.4	24.4	17.1
		2010	19.3	18.8	22.6	32.9	22.0	8.2	6.5	14.2	13.9	16.7	19.8	25.9
		2011	24.1	23.5	27.6									
250 m	U	2009							−2.0	−11.3	−10.7	−10.6	−15.5	−20.2
		2010	−16.2	−7.7	−15.2	−12.6	−5.1	−1.2	−1.4	−7.3	−3.0	−6.2	−12.6	−15.3
		2011	−14.7	−9.5	−16.2									
	V	2009							4.4	13.3	21.9	17.0	17.9	12.9
		2010	14.9	12.4	21.0	25.3	17.1	3.0	2.5	7.0	8.4	12.5	13.8	20.7
		2011	18.2	15.5	21.0									
296 m	U	2009							1.2	−8.9	−8.5	−6.3	−9.6	−14.7
		2010	−10.6	−4.5	−13.4	−9.6	−3.0	−0.6	0.1	−4.9	−1.3	−4.9	−8.7	−11.9
		2011	−10.8	−6.5	−11.7									
	V	2009							1.8	8.3	19.3	11.2	14.2	10.4
		2010	11.9	7.3	18.4	21.4	12.6	−0.9	−0.9	3.8	7.4	10.6	10.8	16.6
		2011	13.7	8.6	15.6									

2008 [*Yuan et al*., 2012a]; (2) the western branch of Kuroshio flows northwestward (or northward) through the upper layer at section 120°40′E between 20°20′N and 21°00′N in the LS during October 2008 [*Yuan et al*., 2012b]. Based on these findings, the mooring station N2 site (Figure 1) is scientifically chosen in the present study to investigate the Kuroshio intrusion.

The present study has three objectives. The first is to describe the time-varying velocity of subtidal currents above 550 m levels at the N2 mooring station from July 2009 to March 2011 and other data. Especially, we compare the weekly near-surface speed from ADCP at the N2 mooring with the surface geostrophic velocity derived from the AVISO data set. The second objective is to analyze the seasonal changes in the Kuroshio intrusion and the variation of the Kuroshio intrusion during El Niño event from July 2009 to April 2010 and La Niña even from June 2010 to March 2011. The third objective is to interpret Kuroshio intrusion dynamics during 2009–2010 El Niño and 2010–2011 La Niña events, supported from the 1/12° global HYCOM model.

2. Data Descriptions

2.1. Currents Observations From the Upper 550 m Obtained at the N2 Mooring Station From July 2009 to March 2011

Mooring station N2 was deployed at 20°40.441′N, 120°38.324′E on 7 July 2009 and retrieved on 20 September 2011 (see Figure 1). An acoustic Doppler current profiler (ADCP) having a maximum observational range of about 600 m was deployed at the nominal depth of 315 m. Sensor position ranged between depths of 315 and 520 m (i.e., shallower depths than the sensors maximum observational range) due to water flow resistance and the drag force exerted on the mooring line. The ADCP therefore collected valid data at depths of 50–300 m with a 30 min sampling interval, from 7 July 2009 to 10 April 2011.

Table 2. Monthly Average Velocities of Subtidal Currents $\vec{v}(550m, m, y)$ as Measured by Aquadopp at Mooring Station N2 for Month (m) and Year (y), From 7 July 2009 to 8 January 2011

	Year	Jan	Feb	Mar	Apr	May	Jun	Jul	Aug	Sep	Oct	Nov	Dec
U	2009							1.0	−2.2	−3.2	1.6	1.1	−2.7
	2010	−2.6	1.7	−6.8	−1.8	1.4	3.5	1.0	1.0	1.9	−7.0	−4.3	−4.5
	2011	−1.5											
V	2009							−1.5	−0.1	6.3	1.5	2.1	1.0
	2010	3.0	−2.5	6.7	11.3	1.9	−9.7	−7.4	4.1	3.9	2.9	3.4	5.3
	2011	3.1											

An additional Aquadopp deep water current meter (hereafter Aquadopp) was deployed at a nominal depth of 534 m. Instrument status, pressure, temperature, and mean current velocities were recorded every 10 min as the sensor was advanced by mooring line between depths of 534 and 746 m, synchronized approximately with the ADCP sensor position, and at an average depth of 550 m throughout the observation period. Aquadopp collected valid data over an 18 month period from 7 July 2009 to 8 January 2011.

In order to construct the subtidal currents, data were processed first with a 40 h Chebyshev Type II digital low-pass filter to remove the tidal signal. Figure 2 shows progressive vector diagrams of observed daily subtidal currents at different depths (tidal signal removed). Tidal characteristics at depths above 550 m as measured at mooring station N2 during the observation period will be presented in a subsequent paper.

2.2. Wind Field Data

The Seaflux data system (JPL; NASA/NOAA) provided wind velocity field data for the study area over the relevant observational period (courtesy of W. Timothy Liu and Wenqing Tang). Figures 3a and 3b show the average wind stress (N/m^2) distribution in the study area for December 2009 and January 2010, respectively. These results show that the average winter wind fields were dominated by strong northeasterly monsoon winds. The average southwestward wind stress is about 0.2 N/m^2 during both months. Figures 3c and 3d show the same wind stress distribution for December 2010 and January 2011, respectively. All of these winter wind stress patterns show very similar northeasterly monsoon signature with southwestward wind stress to be about 0.2 N/m^2.

3. Analysis of Kuroshio Intrusion From Observations

3.1. Analysis of Kuroshio Intrusion From the Subtidal Currents Above 300 m Levels at the N2 Mooring Station

In order to investigate the Kuroshio dynamics using the N2 mooring station data. We began our analysis with the following formulas for current velocities:

$$\vec{v}^M(m,y)=\frac{1}{250}\int_{50}^{300}\vec{v}(z,m,y)dz \quad (1)$$

$$q=q(m,y)=\int_{50}^{300}U(z,m,y)dz \quad (2)$$

$$\vec{v}^N(z)=\frac{1}{N}\sum_{i=1}^{N}\vec{v}(i,z) \quad (3)$$

where $\vec{v}(z,m,y)$ is the monthly average velocity of subtidal currents at depth z for a given month (m)

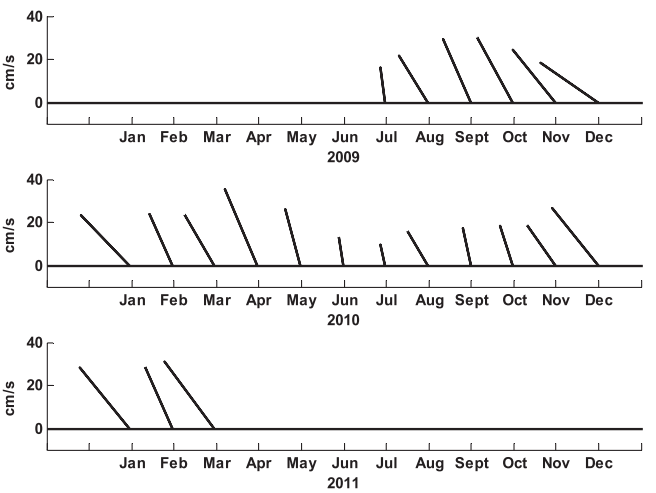

Figure 4. The monthly average current velocities $\vec{v}^M(m,y)$ at 50–300 m depth, as measured at mooring station N2. (top) 2009 data, (middle) 2010 data, and (bottom) 2011 data.

Table 3. Average Volume Transport, q(m, y), of the Kuroshio Intrusion in Month (m) and Year (y) Across a Unit-Length Section at Mooring Station N2, Between Depths of 50 and 300 m (Unit: $m^2 \cdot s^{-1}$)

Year	Jan	Feb	Mar	Apr	May	Jun	Jul	Aug	Sep	Oct	Nov	Dec
2009							−5.5	−34.0	−31.1	−42.5	−50.5	−66.7
2010	−57.5	−27.2	−36.4	−38.5	−17.8	−4.7	−5.7	−24.6	−9.0	−14.6	−34.5	−53.8
2011	−59.0	−32.9	−59.0									

month and year (y) (see Tables 1 and 2); $\vec{v}^M(m, y)$ are the monthly average velocities in the layer at depths of 50–300 m (Figure 4). In formula (2), $U(z, m, y)$ is the east-west component of observed, daily subtidal currents at depth z, for a given month (m) and year (y); positive refers to eastward velocity while negative refers to westward. The term $q(m, y)$ refers to the average VT for the westward Kuroshio intrusion across a unit-length section from depths of 50 to 300 m ($q(m, y) < 0$; see Table 3), at N2 and for a given time frame (m, y). In formula (3), $\vec{v}^N(z)$ shows the average velocities at different depths around mooring station N2 throughout the whole study period (7 July 2009 to 31 March 2011). Figure 5 shows that the average currents all flow northwestward at depths above 550 m, which is the primary upper ocean trend of the Kuroshio current in the vicinity of mooring station N2, and decreases with depths during the observation period.

3.1.1. Seasonal Changes in the Kuroshio Intrusion

Mooring station N2 recorded the Kuroshio intrusion as east-west components in subtidal currents from 7 July 2009 to 31 March 2011. Table 3 lists the associated monthly transport $q(m, y)$. The seasonal variation of transport from Table 3 shows that the strongest Kuroshio intrusion occurred in the winter (December, January, and February), with successively weaker currents in spring (March, April, and May), autumn (September, October, and November), and summer (June, July, and August).

3.1.2. Variation of the Kuroshio Intrusion During El Niño Event From July 2009 to April 2010 and La Niña Event From June 2010 to March 2011

During the winter months, strong, northeasterly monsoon winds affect the study region. The winter Kuroshio intrusion occurs all the time in the LS regardless of what type of ENSO events [e.g., *Metzger and Hurlburt*, 1996; *Caruso et al*., 2006]. However, the strength and dynamics of the Kuroshio intrusion differ. The period from July 2009 to April 2010 marked an El Niño event (referred to as period-E) with a subsequent La Niña event from June 2010 to March 2011 (referred to as period-L; see following Figure 12 in section 4). The current velocities for these events were designated by setting $\overline{q(m,\ y)}\ |_E$ equal to the average value of $q(m, y)$ during period-E, and $\overline{q(m,\ y)}\ |_L$ to the average value of $q(m, y)$ during the period-L. This leads to $-39.0\ m^2\ s^{-1}$ (westward) and $-29.8\ m^2\ s^{-1}$ (westward) as the average $q(m, y)$ in the period-E and period-L (Table 3), respectively. The relative difference between $\overline{q(m,\ y)}\ |_E$ and $\overline{q(m,\ y)}\ |_L$ is 29.8%, indicating consistently higher $q(m, y)$ during El Niño years relative to La Niña years. These results are consistent with the interannual variation presented in previous studies [e.g., *Qu et al*., 2004, 2009; *Yuan et al*., 2012a].

We further examine the maximum absolute intrusion velocity ($|U_{max}(z)|$) for the monthly zonal velocity ($|U(z)|$) during period-E and period-L winters at each observed depth. We define $\Delta_{max}(z)$ as follows:

$$\Delta_{max}(z) = \frac{|U_{max}(z)|_E - |U_{max}(z)|_L}{|U_{max}(z)|_E} \tag{4}$$

where $\Delta_{max}(z)$ is the relative difference in the maximum absolute value of monthly zonal velocity $|U_{max}(z)|$ during period-E ($|U_{max}(z)|_E$) or period-L ($|U_{max}(z)|_L$) at each observed depth z. From formula (4), Table 1 and Figure 6 show the relative difference $\Delta_{max}(z)$ at each observed depth.

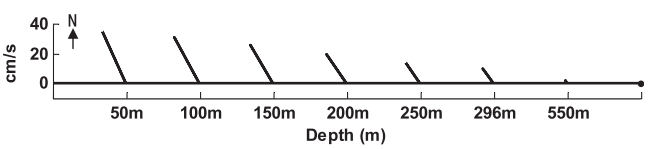

Figure 5. The average velocities $\vec{v}^N(z)$ observed for daily subtidal currents $\vec{v}(i, z)$ during the observed period at the depths of 50, 100, 150, 200, 250, 296, and 550 m of mooring station N2 (see formula (3) in text).

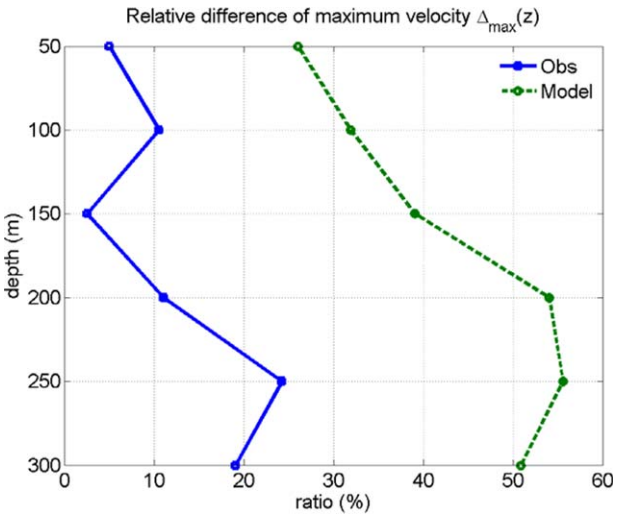

Figure 6. Comparison of relative differences in the maximum absolute velocity of the west directed current component (Δ_{max} (z)) between observations and model results for different depths (z).

Interestingly, these relative differences are increasing with increasing depth, e.g., 5.0% at 50 m, 11.1% at 200 m, and 19.1% at 296 m.

In summary, the above data show that $\Delta_{max}(z) > 0$ across all observed depths, indicating that the Kuroshio intrusion was indeed stronger during period-E than period-L. The data also show that the relevant differences $\Delta_{max}(z)$ in deeper depths were larger than those near the surface. This finding demonstrates that the relative difference in the strength of the Kuroshio intrusion between period-E and period-L is greater in deeper layers of the strait than at the surface. The subsurface maximum due to the ENSO-induced Kuroshio intrusion can be explained as follows. During both period-E and period-L, the average winter wind fields were dominated by strong northeasterly winter monsoon winds. The strong northeasterly monsoon winds exert primary controls on transport variability of the Kuroshio intrusion in the surface layer during both these periods. The relative differences, $\Delta_{max}(z)$,

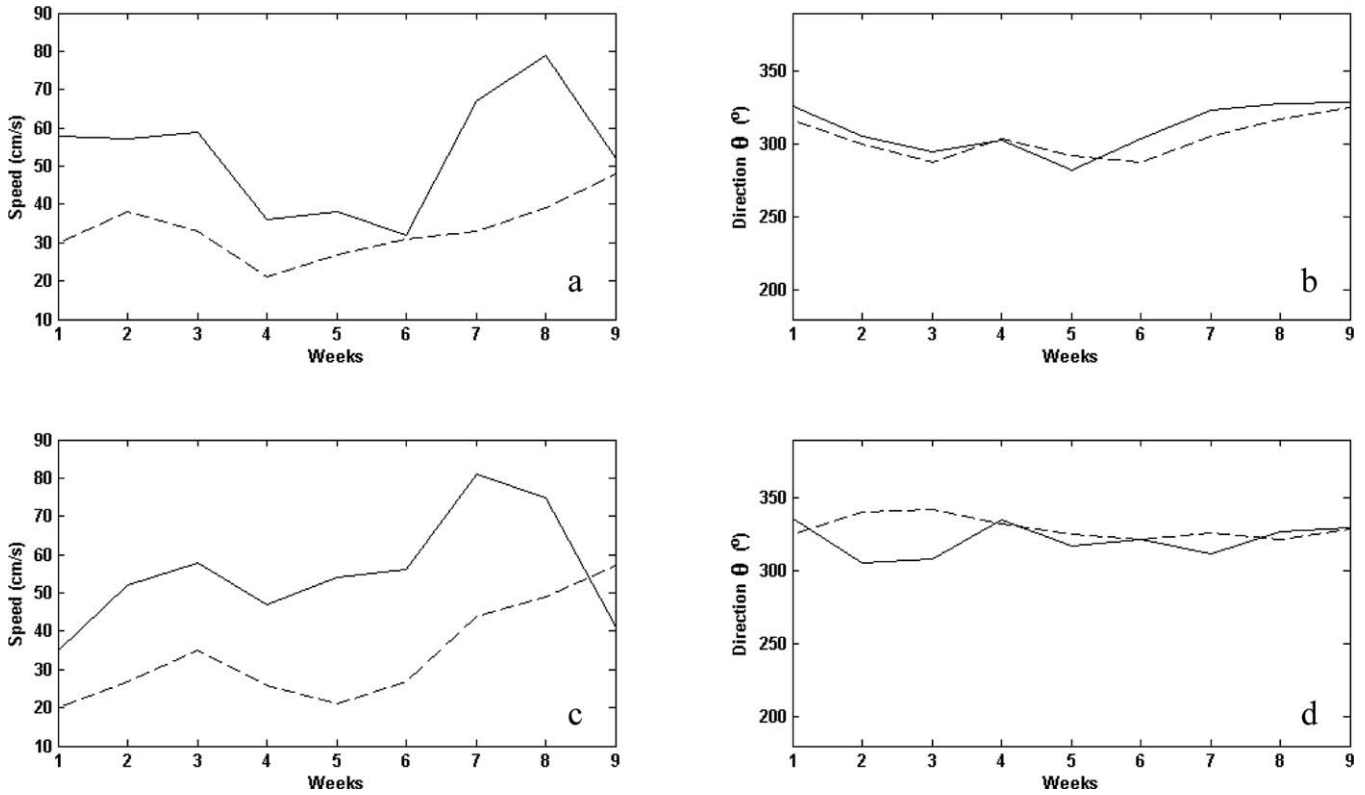

Figure 7. Comparison of the weekly near-surface speed (unit: cm/s) and direction $\bar{\theta}$ (clockwise from north, unit: degree) from ADCP at the N2 mooring (solid lines), as well as the surface geostrophic velocity derived from the AVISO data set (dashed lines) during (a and b) a 9 week period from 2 December 2009 (week 1) to 27 January 2010 (week 9) and (c and d) a 9 week period from 1 December 2010 to 26 January 2011.

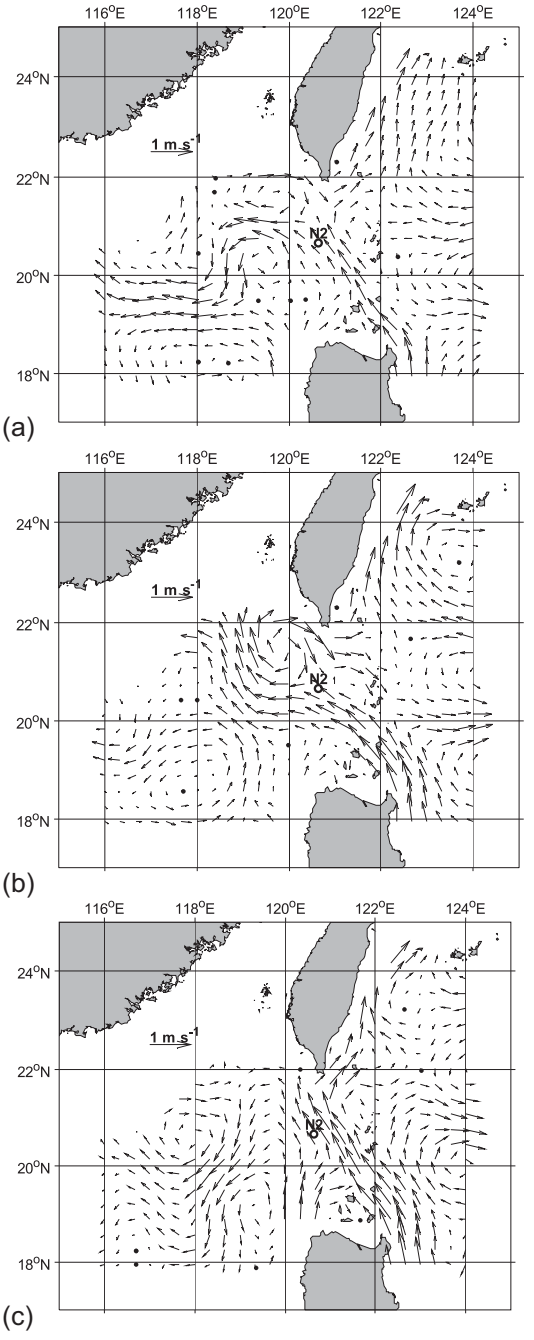

Figure 8. Vectors for geostrophic currents (cm/s) calculated from the merged absolute dynamic topography. The data over the shelf regions of less than 500 m were masked to exclude tidal signals and internal waves. Data shown for (a) 2 December 2009, (b) 30 December 2009, and (c) 27 January 2010.

are therefore not larger in the surface layer. In the subsurface layer however, the impact of northeasterly monsoon winds is reduced rapidly with increasing depth. Under these circumstances, ENSO exerts the dominant effect on the Kuroshio intrusion due to inertial effects that only apply to period-E [see *Masumoto and Yamagata*, 1991; *Qu et al.*, 2004]. The ENSO-induced Kuroshio intrusion therefore exhibits a subsurface maximum.

3.2. Analysis of the Subtidal Currents at 550 m Depth

The characteristic of subtidal currents at 550 m depth for the July 2009 to January 2011 study period are presented in Figure 2d. The overall average velocity is mainly northwestward as expected (Figure 5). Monthly velocity vectors are tabulated in Table 2. In July and August 2009, the observed daily subtidal currents are dominated by anticyclonic flows. The observed daily subtidal currents flow primarily northwestward with monthly average $\overrightarrow{v}(550m, m, y) = (\mathrm{U},\ \mathrm{V}) = (-3.2,\ 6.3)$ in September 2009 (Table 2). The unit is cm/s. From October to December 2009, the observed daily subtidal currents are then dominated by cyclonic flows. After January 2010, the observed daily subtidal currents return to anticyclonic flows until July 2010. During this period, the currents move in a primarily northwestward direction in March and April. From August to November 2010, the observed daily subtidal currents are again dominated by cyclonic movement similar to October to December 2009. Finally, the observed daily subtidal currents flow is mainly northwestward in December 2010.

These results show considerable variation of the daily subtidal currents at 550 m depth between 7 July 2009 and 8 January 2011. Daily subtidal currents oscillate between anticyclonic behavior from July to August 2009 and cyclonic behavior from October to December 2009. The average velocity $\overrightarrow{v}^{N}(550m)$ at 550 m is significantly lower than that at shallower depths and flows in a northwestward direction.

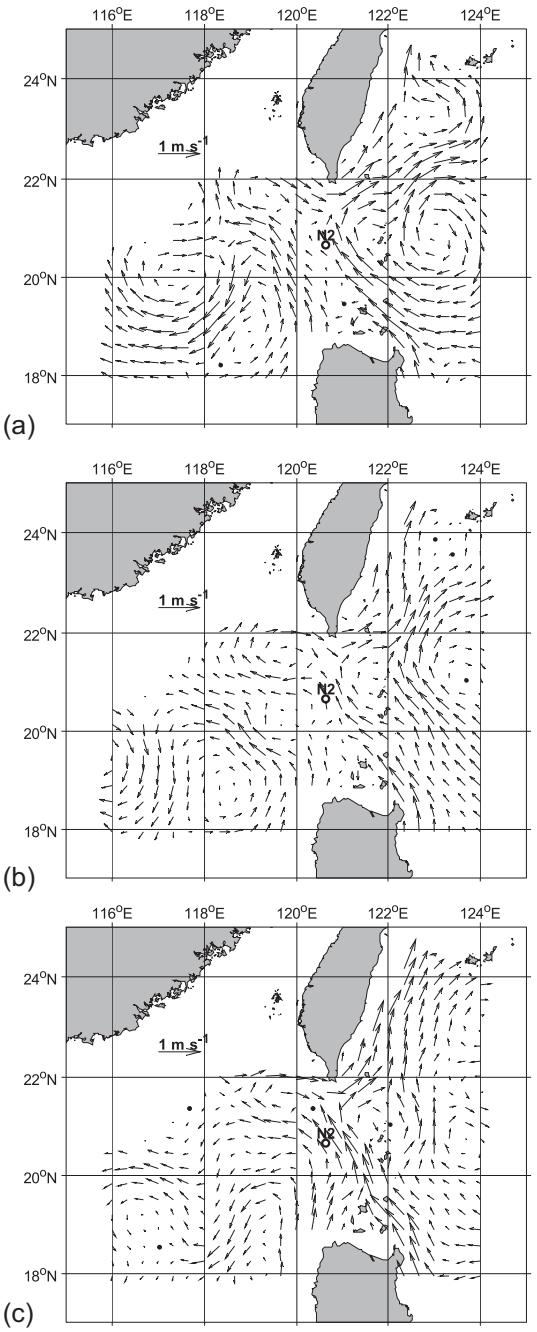

Figure 9. Vectors for geostrophic currents (cm/s) calculated from the merged absolute dynamic topography. The data over shelf regions of less than 500 m depth were masked to exclude tidal signals and internal waves. Data shown for (a) 1 December 2010, (b) 22 December 2010, and (c) 19 January 2011.

3.3. Analysis of Kuroshio Intrusion From Surface Geostrophic Currents and Argo Float Trajectory

Surface geostrophic currents can be used to verify the Kuroshio intrusion in the LS. This section describes surface geostrophic currents for the winters of 2009–2011, along with a trajectory of the Argo float 5 monitored during the 2010–2011 winter. Surface geostrophic currents were interpreted from the merged absolute dynamic topography (ADT) of the sea surface in the study area (Figures 8 and 9). Weekly averaged data were downloaded from the CNES Archiving, Validation, and Interpolation of Satellite Oceanographic Data (AVISO) project using the mapping methods by *Ducet et al.* [2000]. The ADT consists of the mean dynamic topography (MDT) and the sea level anomalies. Details about the MDT estimation are described in *Rio and Hernandez* [2004]. The data for shelf regions shallower than 500 m were masked from analysis due to significant variation from tides and internal waves.

In order to further analyze the Kuroshio intrusion in the AVISO data, we must first validate the AVISO velocity maps according to the following comparisons.

1. We compare the surface geostrophic velocity derived from the AVISO data set with the weekly ADCP near-surface speed and direction (θ) at the N2 mooring for two 9 week periods. One is from 2 December 2009 to 27 January 2010 (referred to as period-E) and the other is from 1 December 2010 to 26 January 2011 (referred to as period-L). Because the AVISO data grids are not colocated with the mooring station N2, we must interpolate the geostrophic velocities at this station based on four neighboring points. Figure 7 and Table 4 show that the weekly ADCP near-surface speeds (***V***) at the N2 mooring station are generally greater than those derived from the AVISO data set. Their relative mean difference was 37% during the period-E, and 38% during the period-L. However, the temporal variation in the weekly speeds (***V***) was qualitatively similar. The weekly ADCP near-surface

Table 4. Comparison of Mean Weekly Near-Surface Speed $\bar{V}$, Eastern Component $\bar{u}$, Northern Component $\bar{v}$(cm/s), and Direction $\bar{\theta}$ (Measured in Degrees Clockwise From North) From ADCP at the N2 Mooring, as Well as the Surface Geostrophic Velocity Derived From the AVISO Data Set During a 9 Week Period From 2 December 2009 (Week 1) to 27 January 2010 (Week 9), and a 9 Week Period From 1 December 2010 to 26 January 2011

Mean Weekly Near-Surface Speed $\bar{V}$, Eastern Component $\bar{u}$, Northern Component $\bar{v}$, and Direction $\bar{\theta}$		Mean Speed $\bar{V}$	Mean Direction $\bar{\theta}$	Mean Eastern Component $\bar{u}$	Mean Northern Component $\bar{v}$
Mean value during a 9 week period from	ADCP	51	313	−37	35
2 Dec 2009 to 27 Jan 2010	AVISO data	32	306	−26	19
Mean value during a 9 week period from	ADCP	55	320	−35	42
1 Dec 2010 to 26 Jan 2011	AVISO data	34	330	−17	29

directions (θ) are mostly northwestward, similar to those derived from the AVISO data set. The difference of their mean weekly directions ($\bar{\theta}$) is 7° during period-E, and 10° during period-L.

2. We compare the zonal (u) and meridional (v) components of the near-surface velocities during period-E and period-L. Table 4 indicates that the mean western component ($\bar{u}$) during period-E is greater than that of period-L in both ADCP and AVISO data, which is consistent with $\Delta_{max}(z=50m) > 0$. This indicates the Kuroshio intrusion is stronger during period-E than during period-L. On the other hand, the mean speed ($\bar{V}$) and mean northern component ($\bar{v}$) during period-L are both greater than those occurring during period-E. The consistency of results from both ADCP and AVISO data suggest that the upstream Kuroshio is stronger during period-L than during period-E. This is because the following cause. The northward shift of the NEC bifurcation is associated with weaker upstream Kuroshio transport during period-E, relative to the southern shift, which is associated with stronger upstream Kuroshio transport during period-L [*Qiu and Lukas*, 1996; *Kim et al*., 2004; *Masumoto and Yamagata*, 1991; *Qu et al*., 2004].

3.3.1. Surface Geostrophic Currents for the Winter of 2009–2010

A relatively strong El Niño event occurred during the 2009–2010 winter (period-E, see the following Figure 12 in section 4), and a strong Kuroshio current that flowed northwest-westward through the LS, between 20°30′N and 21°25′N. This current, referred to as a southern intrusion [*Caruso et al*., 2006], bifurcated near 119°00′E, 21°30′N (Figure 8a). The main current of the intrusion flowed westward at relatively high velocities, reaching 119°00′E and then turning southwestward. The current finally turned westward again to travel across the longitudinal section 118°00′E at approximately 20°N. The other branch of the intrusion looped back eastward just south of 22°N and east of 118°30′E. Over the next 2–4 weeks, the Kuroshio intrusion flowed northwestward at relatively high velocity, reaching an area east of 118°E and south of 22°N, and then bifurcating. The main part of intrusion flowed northwestward toward an area at about 118°00′E and 22°N (Figure 8b). Figure 8b shows the other branch of the intrusion, moving at relatively high velocities and looping back eastward from an area northeast of the main intrusion. By 20 January, an elongated anticyclonic eddy with relatively high velocities that detached from the main intrusion around 117°50′E. Its center was located at about 118°35′E, 21°15′N. By 27 January 2010, this anticyclonic eddy moved southwestward along the shelf break, to a position centered at 118°00′E, 20°30′N (Figure 8c). By this date, the Kuroshio intrusion flowed southwestward through 118°00′E to an area south of the anticyclonic eddy (Figure 8c). The

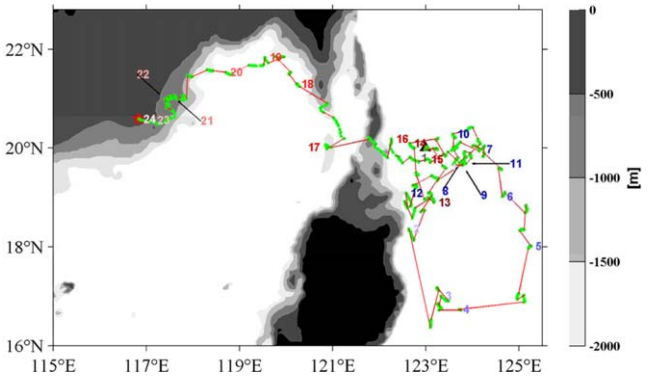

Figure 10. Argo 5 trajectory from 9 July 2009 to 9 June 2011. The triangle symbol refers to the float's initial 9 July 2009 position and the star symbol to its final 9 June 2011 position. Numbers refer to location dates. (1) 9 July 2009; (2) 28 August 2009; (3) 27 September 2009; (4) 27 October 2009; (5) 26 November 2009; (6) 26 December 2009; (7) 25 January 2010; (8) 24 February 2010; (9) 26 March 2010; (10) 25 April 2010; (11) 25 May 2010; (12) 24 June 2010; (13) 24 July 2010; (14) 23 August 2010; (15) 22 September 2010; (16) 22 October 2010; (17) 1 December 2010; (18) 31 December 2010; (19) 30 January 2011; (20) 19 February 2011; (21) 31 March 2011; (22) 20 April 2011; (23) 30 May 2011; (24) 9 June 2011. Green lines with dots represent surface measurements and red lines represent measurements at 1000 m depth.

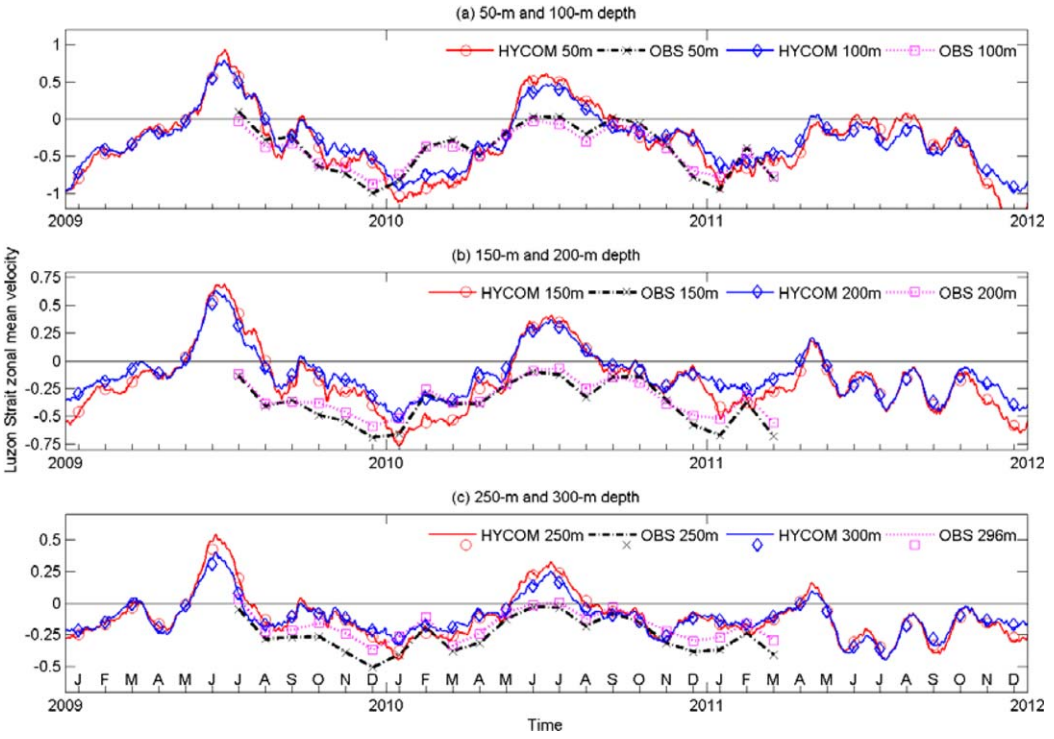

Figure 11. The zonal mean current velocity in the Luzon Strait (from 19.5°N to the southern tip of Taiwan at 120.620°E) at different depths from the 1/12° global HYCOM model. Velocity observations from mooring station N2 are also shown superimposed on model data (lines with × and square symbols). Velocities shown for (a) 50 and 100 m depth, (b) 150 and 200 m depth, and (c) 250 and 300 m depth. A 31 day moving average has been applied to the daily zonal velocity to remove higher frequency variations. Monthly mean data (circle and diamond) are also labeled. The observed velocity is normalized by 40 cm/s and the modeled velocity is normalized by 10 cm/s.

Kuroshio intrusion thus developed into a northern intrusion [after *Caruso et al.*, 2006] by 27 January 2010 (Figure 8c). The evolution of the Kuroshio intrusion through the winter of 2009–2010 resembles intrusion patterns observed for the 1997–1998 winter [*Caruso et al.*, 2006].

3.3.2. Surface Geostrophic Currents for the Winter of 2010–2011

The 2010–2011 winter experienced a La Niña event in December 2010 (period-L, see the following Figure 12 in section 4). From 1–15 December, a weak Kuroshio intrusion flowed northwestward through the LS at around 20°50′N. Most of the current then looped back eastward toward an area south of 22°N and east of 118°00′E (Figure 9a). By 22 December 2010, the Kuroshio current formed a relatively weak southern intrusion [*Caruso et al.*, 2006], flowing northwest-westward through the LS between 20°40′N and 21°20′N. The intrusion then bifurcated near 21°20′N (Figure 9b) with the main branch flowing westward toward 117°00′E, and then turning to flow south at around 21°N. The other branch of the intrusion looped back eastward in an area north of 21°N and east 117°30′E to form a weak anticyclonic eddy (Figure 9b). By 19 January 2011, a weak Kuroshio intrusion flowed northwest-westward through the LS at around 20°50′N and 21°30′N and bifurcated near 21°10′N (Figure 9c). Part of the intrusion then flowed westward toward an area just east of 118°00′E, and then turned southwest-westward and moved toward an area south of 21°10′N. Another part of the intrusion looped back eastward at around 21°10′N and 118°00′E, forming a weak, anticyclonic eddy. The 26 January 2011 current patterns resemble those observed on 19 January 2011 (Figure 9c).

The El Niño winter patterns significantly differed from those in the La Niña winter. During the 2009–2010 El Niño event, the stronger Kuroshio intrusion flowed northwestward through 118°00′E and formed an anticyclonic eddy detached from a loop current in early January. The eddy transited southwestward along the shelf break (Figure 8). During the 2010–2011 La Niña event, however, a weaker Kuroshio intrusion does not flow northwestward through 118°00′E. The intrusion does form a weak anticyclonic eddy after 22 December 2010, but this feature does not detach (Figure 9). The different intrusion strengths between El Niño and La Niña events agree with the observations from mooring station N2. This conclusion is also consistent with

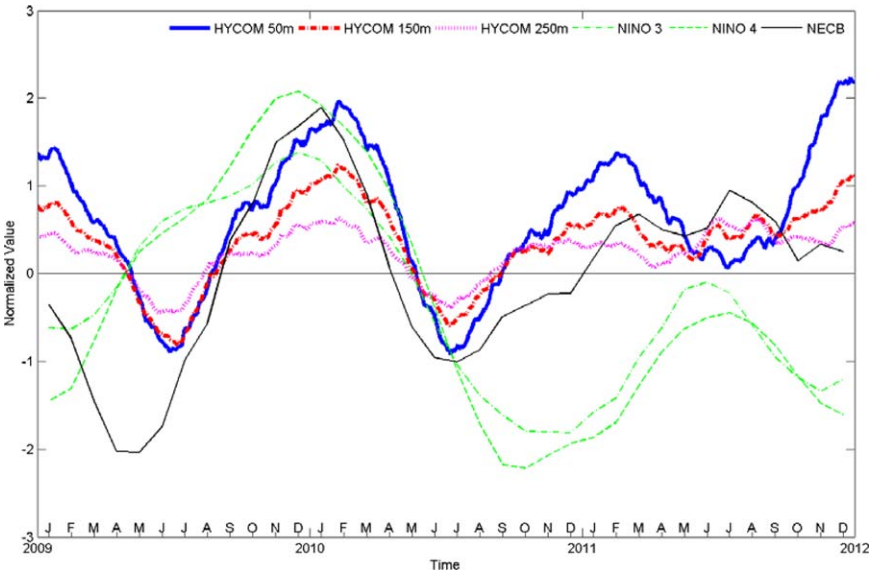

Figure 12. The zonal mean current velocity at different depths in 2009–2012 calculated in HYCOM (91 day moving average has been applied). Niño3, Niño4, and NEC bifurcation latitude indices are shown for comparison. The modeled velocity is normalized by 5 cm/s.

the above comparison of velocities and their zonal and meridional components during periods of 9 weeks-E to periods of 9 weeks-L whether from ADCP or AVISO data.

3.3.3. Trajectories of Argo Float 5 During the 2010–2011 Winter

Argo float 5 was deployed for this study at a position of 20°00′N, 123°0′E on 8 July 2009 (Figure 10). *Yuan et al*. [2014] provided some information about Argo floats 1 through 4. In Figure 10, the green lines with circular dots show that the Argo float 5 move at the surface on 1 day, then it descend to a depth of 1000 m and continue to move at that depth (the red lines) for 10 days. The Argo 5 trajectory can be subdivided into three stages (Figure 10).

During the first period, from 8 July 2009 to 25 January 2010, Argo 5 followed a large-scale cyclonic path at 1000 m depth in an area from about 16°20′ to 20°00′N, and 122°45′ to 125°20′E. Surface currents carried Argo 5 eastward, and upon its descent to 1000 m it then moved south at depth. Argo 5 continued southward with the southward flowing Luzon Undercurrent (LUC) reaching an area south of 17°00′N by mid-October 2009. It then turned eastward, moving at around depths of 1000 m, carried by eastward flow beneath the North Equatorial Undercurrent (NEUC or NEC). After about 1 month and still moving at around 1000 m, Argo 5 turned northward or northeastward with the NUEC, just west of 125°30′E and reached position 7 on 25 January 2010 (see Figure 10).

During the second stage of its trajectory, from 26 January to 10 November 2010, Argo 5 followed a complex path influenced by active, intermediate-scale eddies in the vicinity of 19°10′ to 20°10′N and 122°20′to 124°10′E (see Figure 10).

The final and most important stage of Argo 5's trajectory began at label 17 and lasted from 1 December 2010 to 9 June 2011. During this stage, the Argo 5 trajectory confirms the northwestward Kuroshio intrusion through the LS during the 2010–2011 winter. From December 2010 to January 2011, the stronger northeasterly winds prevailed causing northwestward Ekman drift (see Figures 3c and 3d), and pushing Argo 5 westward across the LS from November 2010 to 30 January 2011.

4. Analysis of Kuroshio Intrusion Dynamics Based on the 1/12° Global HYCOM Model

Section 3 indicates the LS and SCS were influenced by strong northeasterly monsoon winds during both period-E and period-L. Although the Kuroshio intruded westward through the LS during both periods, the observed circulation patterns demonstrate that the intrusion was stronger during the period-E than the

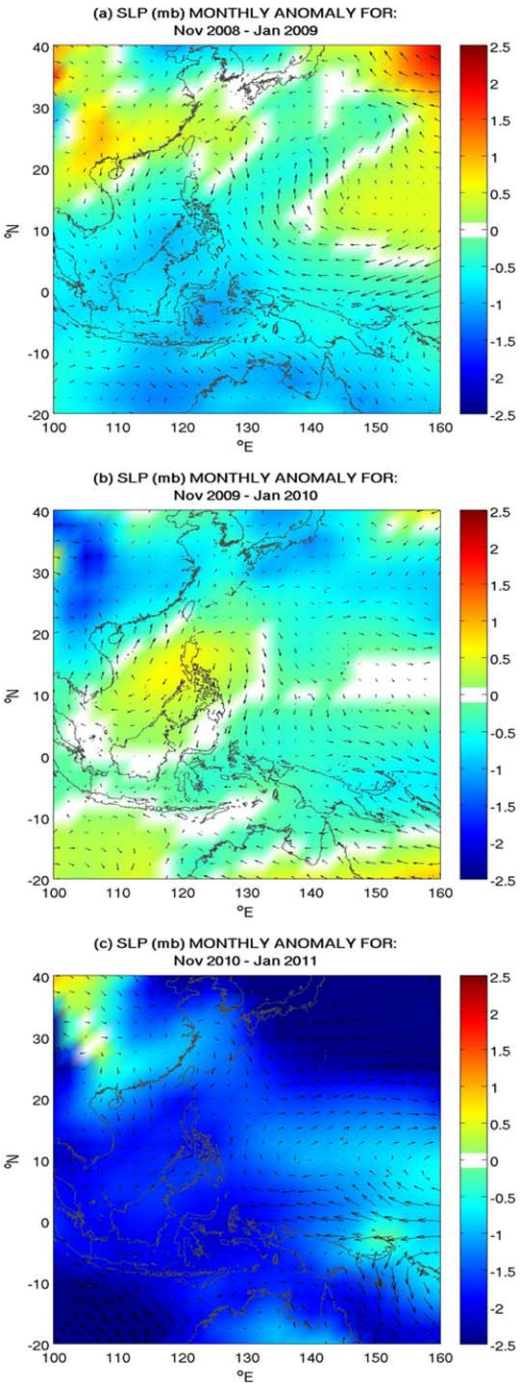

Figure 13. The mean sea level pressure and surface wind anomalies (relative to a period from 1982 to 2011) for three different northern hemisphere winters: (a) November 2008 to January 2009 (normal year), (b) November 2009 to January 2010 (El Niño), and (c) November 2010 to January 2011 (La Niña).

period-L. Here, the 1/12° global HYCOM model results are used to further investigate the dynamics of the Kuroshio intrusion for the same observational periods.

4.1. The 1/12° Global HYCOM Model Configuration

The high-resolution HYCOM provides an appropriate modeling framework for simulating basin-scale circulation like the SCS [*Wang et al*., 2009]. HYCOM data are daily assimilative global results from the HYCOM consortium. HYCOM uses three kinds of vertical coordinates: z-level, terrain-following, and isopycnic [*Bleck*, 2002]. The data subdivide ocean depths into 32 vertical zones covered at a resolution of about 7 km. The quality-controlled bathymetric data from the Naval Research Laboratory's Digital Bathymetry Data Base 2 (NRL DBDB2) are used. The surface forcing, including wind stress, wind speed, heat flux, and precipitation, comes from the Navy Operational Global Atmospheric Prediction System (NOGAPS).

4.2. Kuroshio Intrusion in the 1/12° Global HYCOM

Qu et al. [2004] have shown that LST tends to be higher during El Niño years and lower during La Niña years, with maximum and minimum transport values preceding mature stages of El Niño and La Niña, respectively, by 1 month. Figure 11 shows HYCOM-simulated zonal velocity within the LS from 2009 to 2011 at different depths. A 31 day moving average has been applied to the daily zonal velocity at all depths to remove higher frequency variations. We averaged the zonal velocity laterally from 19°30′N to the south of Taiwan along 120°37.2′E longitude to represent the mean LST velocity. The westward intrusion is shown by the negative zonal mean velocity. Monthly mean data (circle and diamond in Figure 11) are also labeled for comparison with monthly observation from mooring station N2. Figure 11 shows clear seasonal variation of the Kuroshio intrusion at all depths [*Qu et al*., 2004], with a stronger intrusion in the winter and a weaker intrusion in the summer. These results from the winter monsoon forcing described earlier. Interannual variability is also evident in the

subsurface velocity fields down to 300 m depth. The modeled variability of the intrusion resembles the empirical observations on both seasonal and interannual scales. The modeled monthly velocity is generally weaker than the observed monthly data. We therefore normalized the observed velocity by 40 cm/s and the modeled velocity by 10 cm/s to emphasize their variability. The maximum absolute velocity of west directed components (Δ_{max} (z)) from both observations and model results showed reasonable agreement across all observed depths z (see Figure 6). Figures 6 and 11 show that the strength of the period-E intrusion exceeds that of the period-L at all depths. The Δ_{max} (z) values for deeper layers exceed those of surface layer.

To highlight the Kuroshio intrusion associated with different processes, Figure 12 shows the monthly zonal velocity at different depths for the period of 2009–2012. Ninety one day moving average is also applied. The figure also shows Niño3, Niño4, and NEC bifurcation latitude indices (see the definition in *Tzeng et al*. [2012]). Note the zonal velocity is normalized by −5 cm/s for all depths in order to match phases and magnitudes with the indices. The modeled zonal velocity shows reasonable agreement with those climate indices, highlighting concurrent impacts of ENSO influence. A larger Kuroshio intrusion velocity can be seen in the period-E than in the period-L for all depths. Note that the seasonal variability still exists while the climate indices are based on annual cycle removed anomaly. The zonal velocity at depths follows the variation of NEC bifurcation latitude better than the Niño indices. This indicates the NEC bifurcation latitude is a more directly linked to the Kuroshio intrusion. The variability of LS intrusion can be explained by the meridional shifting of the NEC bifurcation associated with ENSO [*Qiu and Lukas*, 1996; *Kim et al*., 2004; *Qu et al*., 2004; *Tzeng et al*., 2012]. During mature El Niño (period-E) or La Niña periods (period-L), the latitude at which the NEC bifurcates shifts northward for El Niño or southward for La Niña. During the period-E, the northward shift of the NEC bifurcation causes weaker upstream Kuroshio transport due to the loss of poleward Kuroshio inertia. These conditions then enhance the Kuroshio intrusion across the LS [*Sheremet*, 2001; *Qu et al*., 2004].

Results described above show that the upper 300 m of the water column experienced higher intrusion velocities during the period-E than period-L (see Figures 8 and 9). These differences resulted mainly from the impact of ENSO. In the period-E, both seasonal variability due to monsoon forcing and the weak upstream Kuroshio transport caused by the ENSO contribute to the large amount of Kuroshio intrusion in the LS. In the period-L, the impact of winter monsoon forcing still exists. However, the stronger upstream Kuroshio transport during this period did not allow the Kuroshio to penetrate into the LS deeply due to the southward shift of the NEC bifurcation caused by the La Niña [*Sheremet*, 2001]. The contrasting ENSO impacts therefore resulted in a stronger Kuroshio intrusion during the 2009–2010 winter (period-E) relative to that of the 2010–2011 winter (period-L).

The meridional shift in the NEC bifurcation latitude and its effects on the Kuroshio intrusion arise due to anomalous anticyclonic winds that formed near the northern Philippine Islands in 2009. These winds are a low-level atmospheric circulation pattern associated with the effects of El Niño around the Philippines, but do not occur during La Niña events. Figure 13 shows the mean sea level pressure anomalies (SLPa) and surface wind anomalies (relative to a period from 1982 to 2011) for three different winters: (a) November 2008 to January 2009 (normal year), (b) November 2009 to January 2010 (El Niño), and (c) November 2010 to January 2011 (La Niña). These time frames demonstrate typical SLP under (a) normal conditions, (b) El Niño conditions, and (c) La Niña conditions. The low-level atmospheric anticyclone originates in the fall of an El Niño year, develops rapidly, and shifts eastward over the Philippine Sea during the winter as the El Niño event matures. The anticyclone persists throughout a few seasons and diminishes in the summer [*Wang et al*., 2003; *Wang and Zhang*, 2002]. The anticyclone is associated with positive SLPa values, which do not occur during normal years or La Niña events. Note that the NEC bifurcation latitude almost varies simultaneously with the Niño3 and Niño4 indices on monthly time scales in Figure 12. This demonstrates the direct impact of atmospheric forcing of Figure 13 on the NEC bifurcation latitude.

5. Conclusion

This study reports the observed current data above 550 m depth from ADCP at mooring station N2 in the LS from 7 July 2009 to 31 March 2011. We also compared it with surface geostrophic currents derived from the AVISO data and the trajectory of Argo float 5 during the 2010–2011 winter. The subtidal current data along with the 1/12° global HYCOM model results were used to interpret the variation of Kuroshio intrusion through the LS on seasonal and interannual scales during 2009–2010 El Niño and 2010–2011 La Niña events.

In terms of seasonal variations of the subtidal currents above 300 m depth, the strongest Kuroshio intrusion occurs during winter, with successively weaker currents in spring, autumn, and summer. We also found that the average current velocities for the westward Kuroshio intrusion were 29.8% higher during 2009–2010 El Niño than 2010–2011 La Niña. Comparison of the maximum absolute values for the western components $|U_{max}(z)|$ of monthly average current velocities at each observed depths z showed that the Kuroshio intrusion was stronger during 2009–2010 El Niño winter than during 2010–2011 La Niña winter. These relevant differences $\Delta_{max}(z)$ were greater in the subsurface layer. This is because the impact of northeasterly monsoon winds is reduced rapidly with increasing depth, and in the subsurface layer the ENSO exerts the dominant effect on the Kuroshio intrusion due to inertial effects that only apply to period-E.

Analysis of the flow patterns at 550 m depth shows the associated mean velocity is significantly lower than that at shallower depths, and is mostly northwestward during the study period. However, a large variation is also observed.

Further validation has been conducted by comparing the surface geostrophic velocity derived from the AVISO data set with the weekly ADCP near-surface speed and direction (θ) at the N2 mooring for two 9 week periods. Their relative mean difference was 37% during the period-E, and 38% during the period-L. However, the temporal variation in the weekly speeds ($\boldsymbol{V}$) was qualitatively similar. The difference of their mean weekly directions ($\bar{\theta}$) is 7° during period-E, and 10° during period-L. Comparing the zonal (u) and meridional (v) components of the near-surface velocities during period-E and period-L, we found that the Kuroshio intrusion is stronger during period-E than during period-L in both ADCP and AVISO data, which is consistent with $\Delta_{max}(z=50m) > 0$. On the other hand, the mean speed ($\bar{V}$) and mean northern component ($\bar{v}$) during period-L are both greater than those occurring during period-E.

The Argo 5 trajectory confirmed the northwestward Kuroshio intrusion through the LS during 2010–2011 winters (the La Niña event). The stronger northeasterly winds prevailed causing northwestward Ekman drift, and pushing Argo 5 westward across the LS from November 2010 to 30 January 2011.

These results further supported the finding at mooring station N2 that the Kuroshio intrusion across the LS during 2009–2010 winter (El Niño event) was stronger than that during 2010–2011 winter (La Niña event), consistent with the observation at mooring station N2.

The 1/12° global HYCOM model provided further theoretical bases to support our observational analysis. Modeled variation in the Kuroshio intrusion agreed reasonably well with the observation on both seasonal to interannual scales. The model shows larger $\Delta_{max}(z)$ in the deeper ocean, consistent with the observations. Modeled zonal velocity resembled those of the Niño3, Niño4, and NEC bifurcation latitude indices, affirming the salient influence of ENSO variation in winter. The Kuroshio intrusion velocity observed in the upper 300 m layer from December 2009 to February 2010 exceeded the values observed from December 2010 to February 2011. This result was also evident in the modeled zonal mean velocity in the LS.

Our results indicate that the underlying mechanisms driving the Kuroshio intrusion into the LS differ on seasonal and interannual scales. Monsoon winds strongly affect the seasonal variation while the weak upstream Kuroshio transport induced by El Niño, strongly affects the interannual variation, such as 2009–2010 winter. In 2010–2011 winter, the impact of winter monsoon forcing still exists in the LS. However, the stronger upstream Kuroshio transport during this period did not allow the Kuroshio to penetrate into the LS deeply due to the southward shift of the NEC bifurcation caused by the La Niña event. This explains why the 2009–2010 winter Kuroshio intrusion (El Niño event) was stronger than that of the 2010–2011 winter (La Niña event). Meridional shifting of the NEC bifurcation latitude and the associated shift of the Kuroshio current in the vicinity of the LS resulted from the development of an anomalous anticyclonic wind formed near the northern Philippines in 2009.

Acknowledgments

The wind data are obtained from the NASA/NOAA sponsored data system Seaflux, at JPL through the courtesy of W. Timothy Liu and Wenqing Tang, the authors are grateful to them for their effective wind data. This work was supported by the National Basic Research Program of China (2007CB816003 and 2011CB403503), the International Cooperative Project of the Ministry of Science and Technology of China (2006DFB21630), the Key project of the National Natural Science Foundation of China (40520140073 and 41176020), and grants from the Scientific Research Fund of the SIO, SOA (grant JT1006) and the project of Global Change and Air-Sea Interaction (GASI-03-01-01-02). We also wish to thank the crew and participants of the R/V Dong Fang Hong-2 and the R/V Zhongda-31 for their supports and cooperation.

References

Bleck, R. (2002), An oceanic general circulation model framed in hybrid isopycnic-Cartesian coordinates, *Ocean Modell.*, *4*, 55–88.

Caruso, M. J., G. G. Gawarkiewicz, and R. C. Beardsley (2006), Interannual variability of the Kuroshio Intrusion in the South China Sea, *J. Oceanogr.*, *62*, 559–575.

Ducet, N., P. Y. Le Traon, and G. Reverdin (2000), Global high resolution mapping of ocean circulation from TOPEX/Poseidon and ERS-1/2, *J. Geophys. Res.*, *105*, 19,477–19,498.

Fang, G. H., Y. G. Wang, Z. X. Wei, Y. Fang, F. L. Qiao, and X. M. Hu (2009), Interocean circulation and heat and freshwater budgets of the South China Sea based on a numerical model, *Dyn. Atmos. Oceans*, *47*, 55–72.

Farris, A., and M. Wimbush (1996), Wind-induced Kuroshio Intrusion into the South China Sea, *J. Oceanogr.*, *52*, 771–784.
Kim, Y. Y., T. Qu, T. Jensen, T. Miyama, H. Mitsudera, H.-W. Kang, and A. Ishida (2004), Seasonal and interannual variations of the North Equatorial Current bifurcation in a high-resolution OGCM, *J. Geophys. Res.*, *109*, C03040, doi:10.1029/2003JC002013.
Liang, W.-D., Y. J. Yang, T. Y. Tang, and W.-S. Chuang (2008), Kuroshio in the Luzon Strait, *J. Geophys. Res.*, *113*, C08048, doi:10.1029/2007JC004609.
Liao, G. H., Y. C. Yuan, and X. H. Xu (2007), Diagnostic calculation of the circulation in the South China Sea during the summer 1998, *J. Oceanogr.*, *63*, 161–178.
Liao, G. H., Y. C. Yuan, and X. H. Xu (2008), Three dimensional diagnostic study of the circulation in the South China Sea during winter 1998, *J. Oceanogr.*, *64*, 803–814.
Masumoto, Y., and T. Yamagata (1991), Response of the western tropical Pacific to the Asian winter monsoon: The generation of the Mindanao Dome, *J. Phys. Oceanogr.*, *21*, 1386–1398.
Metzger, E. J., and H. E. Hurlburt (1996), Coupled dynamics of the South China Sea, the Sulu Sea, and the Pacific Ocean, *J. Geophys. Res.*, *101*, 12,331–12,352.
Qiu, B., and S. Chen (2010), Interannual-to-decadal variability in the in the bifurcation of the North Equatorial Current off the Philippines, *J. Phys. Oceanogr.*, *40*, 2525–2538.
Qiu, B., and R. Lukas (1996), Seasonal and interannual variability of the North Equatorial Current, the Mindanao Current and the Kuroshio along the Pacific western boundary, *J. Geophys. Res.*, *101*, 12,315–12,330.
Qu, T. (2000), Upper layer circulation in the South China Sea, *J. Phys. Oceanogr.*, *30*, 1450–1460.
Qu, T. (2002), Evidence for water exchange between the South China Sea and the Pacific Ocean through the Luzon Strait, *Acta Oceanol. Sin.*, *21*, 175–185.
Qu, T., Y. Y. Kim, M. Yaremchuk, T. Tozuka, A. Ishida, and T. Yamagata (2004), Can Luzon Strait transport play a role in conveying the impact of ENSO to the South China Sea?, *J. Clim.*, *17*, 3644–3657.
Qu, T., Y. T. Song, and T. Yamagata (2009), An introduction to the South China Sea throughflow: Its dynamics, variability, and application for climate, *Dyn. Atmos. Oceans*, *47*, 3–14.
Rio, M. H., and F. Hernandez (2004), A mean dynamic topography computed over the world ocean from altimetry, in situ measurements, and a geoid model, *J. Geophys. Res.*, *109*, C12032, doi:10.1029/2003JC002226.
Sheremet, V. A. (2001), Hysteresis of a western boundary current leaping across a gap, *J. Phys. Oceanogr.*, *31*, 1247–1259.
Taniguchi, N., et al. (2010), Long-term acoustic tomography measurement of ocean currents at the northern part of the Luzon Strait, *Geophys. Res. Lett.*, *37*, L07601, doi:10.1029/2009GL042327.
Tzeng, W.-N., Y. H. Tseng, Y. S. Han, C.-C. Hsu, C. W. Chang, E. Di Lorenzo, and C.-H. Hsieh (2012), Evaluation of multi-scale climate effects on annual recruitment levels of the Japanese Eel, *Anguilla japonica*, to Taiwan, *PLoS ONE*, *7*, e30805, doi:10.1371/journal.pone.003080.
Wang, B., and Q. Zhang (2002), Pacific–east Asian teleconnection. Part II: How the Philippine Sea anomalous anticyclone is established during El Niño development, *J. Clim.*, *15*, 3252–3265.
Wang, B., R. Wu, and T. Li (2003), Atmosphere–warm ocean interaction and its impacts on Asian–Australian monsoon variation, *J. Clim.*, *16*, 1195–1211.
Wang, H. Q., Y. C. Yuan, W. B. Guan, C. H. Yang, G. H. Liao, and Z. Y. Cao (2012), Circulation around the Luzon Strait in September as inferred from CTD, Argos and Argo measurements and a generalized topography-following, *Atmos. Ocean*, *50*, suppl. 1, 40–58.
Wang, Q., H. Cui, S. Zhang, and D. Hu (2009), Water transports through the four main straits around the South China Sea, *Chin. J. Oceanol. Limnol.*, *27*, 229–236.
Wu, C.-R., and Y.-C. Hsin (2012), The forcing mechanism leading to the Kuroshio intrusion into the South China Sea, *J. Geophys. Res.*, *117*, C07015, doi:10.1029/2012JC007968.
Yaremchuk, M., and T. Qu (2004), Seasonal variability of the circulation near the Philippine coast, *J. Phys. Oceanogr.*, *34*, 844–855.
Yuan, Y. C., G. H. Liao, and X. H. Xu (2007), Three dimensional diagnostic modeling study of the South China Sea circulation before onset of summer monsoon in 1998, *J. Oceanogr.*, *63*, 77–100.
Yuan, Y. C., G. H. Liao, W. B. Guan, H. Q. Wang, R. Y. Lou, and H. Chen (2008), The circulation in the upper and middle layers of the Luzon Strait during spring 2002, *J. Geophys. Res.*, *113*, C06004, doi:10.1029/2007JC004546.
Yuan, Y. C., G. H. Liao, and C. H. Yang (2009), A diagnostic calculation of the circulation in the upper and middle layers of the Luzon Strait and the northern South China Sea during March 1992, *Dyn. Atmos. Oceans*, *47*, 86–113.
Yuan, Y. C., G. H. Liao, A. Kaneko, C. H. Yang, X.-H. Zhu, H. Chen, N. Gohda, N. Taniguchi, and M. Minamidate (2012a), Currents in the Luzon Strait obtained from moored ADCP observations and a diagnostic calculation of circulation in spring 2008, *Dyn. Atmos. Oceans*, *58*, 20–43.
Yuan, Y. C., G. H. Liao, C. H. Yang, Z.-H. Liu, H. Chen (2012b), Currents in the Luzon Strait evidenced by CTD and Argo observations and a diagnostic model in October 2008, *Atmos. Ocean*, *50*, suppl. 1, 27–39.
Yuan, Y. C., G. H. Liao, C. H. Yang, Z.-H. Liu, H. Chen and Z. G. Wang (2014), Summer Kuroshio Intrusion through the Luzon Strait confirmed from observations and a diagnostic model in summer 2009, *Prog. Oceanogr.*, *121*, 44–59.